Cooperative MIMO-OFDM-Based Exposure-Path Prevention Over 3D Clustered Wireless Camera Sensor Networks

Jingqing Wang and Xi Zhang, *Fellow, IEEE*

***Abstract*— As compared with 2D wireless camera sensor networks (WCSNs), 3D WCSNs can capture more accurate and comprehensive information for exposure-path prevention in supervisory and military applications. However, 3D WCSNs impose many new challenges for energy-efficiency and interference-mitigation subject to required coverage rate constraint due to extensive power consumption over time-varying wireless channels. To overcome the above-mentioned problems, in this paper we propose the AQ-DBPSK/DS-CDMA (alternating quadratures differential binary phase shift keying/direct-sequence code division multiple access) based cooperative MIMO energy-efficient and interference-mitigating scheme under the constraint of optimal tradeoff between power consumption and coverage rate over multi-hop clustered WCSNs. In particular, we build sensing models to characterize the minimum coverage rate constraint and formulate the exposure-path prevention problem using the percolation theory. Then, we derive the critical density of camera sensors subject to minimum exposure-path prevention probability constraint. We develop the AQ-DBPSK/DS-CDMA scheme and also derive the optimal data rate to optimize transmit-power and data-rate trade-off. By deriving the critical density of camera sensors over 3D WCSNs, we apply the cooperative MIMO based NEW LEACH architecture for our multi-hop cooperative MIMO scheme. Also conducted is a set of simulations which show that our proposed scheme can outperform other existing schemes in terms of energy efficiency and interference-mitigation over multi-hop 3D clustered WCSNs.**

***Index Terms*— 3D clustered wireless camera sensor networks (WCSNs), percolation theory, exposure-path prevention, NEW LEACH, multi-hop cooperative MIMO, AQ-DBPSK/DS-CDMA, Nakagami-m channels.**

I. Introduction

A. Backgrounds and Motivations

THE explosive development in VLSI devices and image sensor techniques has enabled the cost effective development of the large-scale, small-size, and energy-saving wireless camera sensor networks (WCSNs). As a result, how to efficiently design and implement WCSNs in many critical applications, such as the battlefield surveillance, homeland security, industrial process supervision, and health monitoring systems has received a great deal of research attention from both academia and industry [1], [2].

One of the key issues in designing and implementing WCSNs is how to optimize the trade-off between power consumption and coverage rate. Most existing works on sensor coverage mainly focus on full coverage models. To remedy this deficiency, researchers have focused on investigating the exposure-path prevention problem [3] with partial coverage. Accordingly, researchers have proposed the percolation theory [4] as a powerful and effective way in solving the exposure-path prevention problem in 2D WCSNs. Although the existing 2D sensing models are analytically more tractable in designing and evaluating the directional WCSNs for coverage-control, they cannot accurately characterize some practical application scenes. Accordingly, research about coverage problem in 3D WCSNs has much more practical significance. While the percolation theory in principle can be potentially extended into 3D models to further improve the power and exposure-path prevention performance, there are still many new challenges remaining unsolved in the 3D WCSNs due to the high complexity in the design and analysis imposed by the 3D sensing model.

On the other hand, the clustering algorithm is widely cited as an effective energy-efficient and interference mitigation technique for 2D WCSNs. There are many existing works on the clustering algorithms [5], [6]. As compared with 2D WCSNs, 3D WCSNs can provide more accurate and comprehensive information for various supervisory applications, thus attracting much more research attention. However, 3D WCSNs also impose many new challenges not encountered in 2D WCSNs, including the high complexity in designing and analyzing the application of clustering techniques in order to implement the energy-efficient and interference-mitigating schemes for 3D WCSNs subject to the minimum coverage rate constraint.

In addition, to improve the energy efficiency, several advanced techniques, such as multiple-input-multiple-output (MIMO) and orthogonal frequency-division multiplexing (OFDM) schemes, have been widely developed and implemented in WCSNs. Furthermore, the combined MIMO-OFDM [7] technique can achieve the advantages of both MIMO and OFDM. However, because of the low-cost small-

Manuscript received December 24, 2018; revised May 31, 2019; accepted July 18, 2019. Date of publication August 12, 2019; date of current version January 8, 2020. This work was supported in part by the U.S. National Science Foundation under Grant ECCS-1408601 and Grant CNS-1205726, and in part by the U.S. Air Force under Grant FA9453-15-C-0423. The associate editor coordinating the review of this article and approving it for publication was M. Li. *(Corresponding author: Xi Zhang.)*

The authors are with the Networking and Information Systems Laboratory, Department of Electrical and Computer Engineering, Texas A&M University, College Station, TX 77843 USA (e-mail: wang12078@tamu.edu; xizhang@ece.tamu.edu).

Color versions of one or more of the figures in this article are available online at http://ieeexplore.ieee.org.

Digital Object Identifier 10.1109/TWC.2019.2933201

sized characteristics of camera sensors, it is impractical to directly apply MIMO scheme in WCSNs. Consequently, researchers have proposed the idea of cooperative MIMO-OFDM [8] scheme as a promising technique for wireless sensor networks. The cooperative MIMO-OFDM technology has been widely applied in various military contexts and applications for significant performance gains in a cost-effective manner. In cooperative WCSNs, camera sensors relay on each others' messages in order to provide spatial diversity and increase the spectral efficiency by combining the received signals at the physical layer. Nevertheless, although the cooperative MIMO-OFDM scheme can potentially improve system performance, a number of new issues may significantly complicate its implementation over 3D WCSNs. For example, how to characterize the inter-cluster and intra-cluster wireless data transmissions for cooperative MIMO-OFDM scheme is still a challenging problem over multi-hop 3D WCSNs.

Furthermore, in order to further improve the energy efficiency, some existing works tackle the simple but robust coding and modulation techniques in WCSNs [9], [10]. The DS-CDMA technique [11], which enables the signals to appear similar to the random noise by using the spreading codes, has been widely applied in various military contexts and applications for its robustness to a wide variety of interferences. Another novel modulation technique called AQ-DBPSK has been proposed and proven to be a simple, robust, and effective modulation scheme enabling much superior energy efficiency over the other modulation schemes, such as binary phase shift keying (BPSK) and differential binary phase shift keying (DBPSK). However, how to efficiently integrate the AQ-DBPSK modulation scheme with the underlaying DS-CDMA framework in 3D clustered WCSNs still remains as an open problem.

To overcome the above-mentioned challenges while optimizing the trade-off between energy efficiency and coverage rate, in this paper we propose a number of designing schemes for 3D WCSNs including the sensor coverage model, communication/routing/clustering system models, advanced modulation techniques, and multiple channel access mechanism to improve the energy efficiency. In particular, we efficiently integrate the AQ-DBPSK/DS-CDMA based cooperative MIMO scheme with the underlaying clustering framework over multi-hop 3D clustered WCSNs in the following steps. First, we establish the sensing models to characterize the minimum coverage rate constraint, formulate the exposure-path prevention problem under the percolation theory, and establish the wireless channel model using Nakagami-m distribution. Second, we derive the critical density of camera sensors subject to the minimum exposure-path prevention probability constraint using bond-percolation theory. Third, to analyze the energy efficiency, we apply the AQ-DBPSK/DS-CDMA technique as an effective way to significantly mitigate the interference among camera sensors, and thus improving the energy efficiency over large scale 3D WCSNs. Accordingly, we propose the optimal rate control policy that maximizes the energy efficiency for AQ-DBPSK/DS-CDMA based 3D WCSNs. Finally, under the minimum exposure-path prevention probability constraint, we apply the critical density when designing the cooperative MIMO based NEW LEACH architecture over 3D WCSNs, which derives the optimal cluster head selection probability that minimizes the average total energy consumption over the entire 3D clustered WCSNs. We also conduct a set of simulations which evaluate the system performances and show that our proposed AQ-DBPSK/DS-CDMA based cooperative MIMO scheme outperforms the other existing schemes under minimum exposure-path prevention probability constraint over clustered 3D WCSNs.

B. The Related Works

As one of the fundamental problems of wireless sensor networks, the coverage problem of the deployed sensors plays an important role in intrusion detection. Unlike the classic full coverage model which requires that every point in the sensor deployed region is covered, the exposure-path problem has been investigated to determine whether an intruder can traverse without being discovered [2]. In order to solve the exposure-path prevention problem, authors in [3] and [12] have applied the percolation theory and derived the optimal density of the deployed camera sensors in 2D WCSNs. Researchers have applied percolation theory [4] to investigate the connectivity of wireless networks. Most previous works have focused on exploiting the percolation theory to derive the optimal density for coverage over 2D WCSNs. However, in some practical scenarios, the sensors are deployed in the space rather than in a planar field to provide with more comprehensive information. For example, 3D camera sensor deployment design for WCSNs is required for sensing/monitoring the trees of different heights in a forest, buildings with multiple floors, and the underwater environment. In our previous work [1], we have extended the exposure-path prevention problem into 3D WCSNs to future improve the power and exposure-path prevention performance. Authors in [13] have investigated the critical density for percolation in coverage and connectivity over 3D wireless sensor networks.

On the other hand, to improve the energy efficiency over WCSNs, in the recent years, researchers have designed various techniques, including the design of low-power signal processing architectures, robust coding and modulation techniques, energy efficient wireless media access control and routing protocols, localization systems [14], energy efficient clustering algorithms, etc. Authors in [5] have proposed a cooperative target localization algorithm, which aims to optimize the tradeoff between the energy consumption of WCSNs and the quality of the target localization. A 3D coverage scheme over WCSNs has been developed in [6] to maximize the lifespan by minimizing the energy consumption subject to the minimum coverage rate. The virtual MIMO communication protocol has been proposed in [8] by using the cross-layer design to jointly improve the energy efficiency, reliability, and end-to-end QoS provisioning in wireless sensor network. Authors in [15] have developed a clustered topology over cooperative distributed MIMO channels for multi-hop wireless sensor networks. Our previous work [16] has proposed the cooperative MIMO-OFDM system over multi-hop 3D clustered WCSNs. In addition, to further improve the energy efficiency, the authors

TABLE I
SUMMARY OF NOTATIONS

Q	Number of multi-paths	$R_{k,s}$	sensing radius
$R_{k,f}$	Blind area radius	θ_k	Offset angle
$\mathcal{P}_k$	Transmit Power at node k	L_k	3D sphere center
L_t	Target center	$d_{k,t}$	Euclidean distance between L_k and L_t
V_k^{o}	Sensing volume for omnidirectional model	V_k^{d}	Sensing volume for directional model
$\overrightarrow{V_k}$	Sensing direction	λ	Sensors distributed density
$\mathbf{V}$	3D sensing space	$2a$	Length of sensing space
λ_c	Critical density of camera sensors	$e_{i,j}$	Edge between vertexes v_i and v_j
$L(e_{i,j})$	Indicator for L-closed/L-open edges	$U(e_{i,j})$	Indicator for U-closed/U-open edges
p_l	probability of L-closed edges	p_u	probability of U-closed edges
$h_{k,n}(t)$	Channel impulse response function	$\tau_{k,n}^{(q)}$	Path delay
$a_{k,n}^{(q)}$	Path envelope	$\phi_{k,n}^{(q)}$	Phase-shift over qth multi-path
$r_{k,n}(t)$	Received signal from node k to node n	f_c	Central frequency
$b\left(t-\tau_{k,n}^{(q)}\right)$	Transmitted symbol from node k to node n	$n_{k,n}(t)$	Complex AWGN
$c\left(t-\tau_{k,n}^{(q)}\right)$	Spread code	P_{T_c}	Unit rectangular-pulse function
T_c	Chip duration	T_s	Symbol duration
N_s	Spread gain	p_c	Percolation threshold
λ_l	Node density for L-coverage lattice	λ_u	Node density for U-coverage lattice
$O_i^{\bigsqcup}$	Volume of $S_i \bigsqcup S_j$	$O_i^{\bigcap}$	Volume of $S_i \bigcap S_j$
λ_c^{o}	Critical density for omnidirectional model	λ_c^{d}	Critical density for directional model
$P_b(\gamma_{k,n})$	Bit error rate	$\gamma_{k,n}^{(q)}$	SNR over qth multi-path
$\eta_{k,n}$	Energy efficiency	ρ_k	Transmit power efficiency
$\mathcal{P}_{k,c}$	Circuit power	$\xi(k)$	CH selection threshold
p_ω	Probability for becoming a CH	P_{out}	Outage probability for L multi-hops

of [9] have investigated the multicarrier DS-CDMA system over the generalized multipath Nakagami-m fading channel. Our previous work [11] has combined the DS-CDMA system with AQ-DBPSK technique for 3D clustered WCSNs subject to coverage rate constraint. The authors in [17] have integrated transmit selection diversity/maximal-ratio combining (TSD/MRC) with multicarrier DS-CDMA.

From aforementioned related works, we can observe that the exposure-path prevention and the optimal critical density that optimize the trade-off between power consumption and coverage probability are still open and challenging problems over 3D WCSNs. To overcome this problem, we propose the cooperative MIMO-OFDM based exposure-path prevention over 3D clustered WCSNs.

C. The Main Contributions of This Paper

Our main contributions in this paper are summarized as follows:

- We develop the exposure-path-prevention schemes for 3D WCSNs, which tackle the problem on how to efficiently apply the cooperative MIMO-OFDM technique subject to the coverage rate constraint over clustered 3D WCSNs.
- Under the minimum exposure-path prevention probability constraint, we derive the critical density of camera sensors and analyze the mutual dependency among neighboring edges to apply the bond-percolation theory into our proposed 3D sensing models.
- To mitigate the interference and improve energy efficiency, we develop the AQ-DBPSK/DS-CDMA scheme over WCSNs and derive the optimal data rate to maximize the energy efficiency.
- Using our derived critical density of camera sensors, we propose and develop the cooperative MIMO-LEACH scheme and derive the optimal cluster-head selection probability that minimizes the average total energy consumption over the entire 3D clustered WCSNs.

The rest of this paper is organized as follows: Section II establishes the sensing models to characterize the minimum coverage rate constraint, the bond-percolation model, and the wireless channel model using Nakagami-m distribution for our proposed 3D WCSNs. Section III formulates the coverage problem to derive the optimal density for exposure-path prevention and measures the mutual dependency among 3D neighboring camera sensors. Section IV develops AQ-DBPSK/DS-CDMA technique to improve the energy-efficiency and interference-mitigation for 3D clustered WCSNs. Section V derives the optimal data rate to maximize the energy efficiency. Section VI combines the cooperative MIMO algorithm with NEW LEACH architecture. Section VII evaluates and compares the performances of our proposed schemes with the other existing schemes. The paper concludes with Section VIII.

Notations: Throughout this paper, the following notations are used. $(\cdot)^T$ represents the transpose of a matrix. $\mathbb{E}[\cdot]$ stands for the expectation. All logarithm functions are based on e, unless otherwise stated. The notations used throughout the paper are summarized in Table I.

II. THE SYSTEM MODELS

Since the viewpoints in 2D WCSNs are restricted to the positions where physical cameras locate, fixed viewpoint surveillance cannot gather all of the necessary information. A 3D view of the scene is more desirable compared with traditional

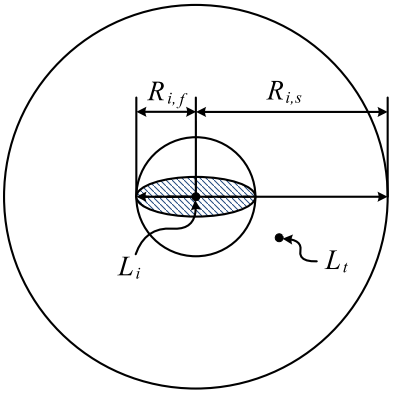

Fig. 1. 3D omnidirectional model for WCSNs.

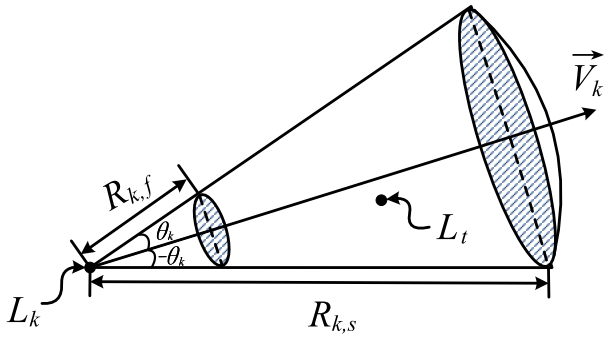

Fig. 2. 3D directional model for WCSNs.

2D surveillance/monitoring. Compared with the traditional 2D camera sensing model, 3D WCSNs are often deployed in the space rather than in a planar field to provide with more comprehensive information for some practical scenarios. For example, 3D camera sensor deployment design for WCSNs is required for sensing/monitoring the battle fields in the mountain areas and monitoring buildings with multiple floors.

There are two types of 3D sensing models: the omnidirectional model and directional model, shown in Fig. 1 and Fig. 2, respectively. Our system models are under the following assumptions:

1) All camera sensors are heterogeneous with different sensing radiuses $R_{k,s}$, different sensing angles $2\theta_k$, and different transmit powers $\mathcal{P}_k$.
2) Each camera sensor uses 1 unit of energy to transmit or receive 1 unit of data.

A. The 3D Sensing Models

1) 3D Omnidirectional Sensing Model:

The 3D omnidirectional model is based on the sphere model for omnidirectional WCSNs. Let $L_k \triangleq (x_k, y_k, z_k)$ represent the location of camera sensor k, $R_{k,s}$ denote the sensing radius, and $R_{k,f}$ be the radius for the blind area. As shown in Fig. 1 [1], the omnidirectional model for a camera sensor is a 3D sphere space centered at L_k. A target point $L_t \triangleq (x_t, y_t, z_t)$ in the 3D space is said to be covered if

$$R_{k,f} \leq d_{k,t} \leq R_{k,s} \tag{1}$$

where $d_{k,t}$ represents the Euclidean distance between L_k and L_t which is defined as follows:

$$d_{k,t} = \sqrt{(x_t - x_k)^2 + (y_t - y_k)^2 + (z_t - z_k)^2}. \tag{2}$$

Accordingly, if the distance between the target and the sensor node is less than $R_{k,f}$, the target cannot be detected. From the omnidirectional model, the sensing volume V_k^{o} is determined as follows:

$$V_k^{\mathrm{o}} = \frac{4\pi\left(R_{k,s}^3 - R_{k,f}^3\right)}{3}. \tag{3}$$

2) 3D Directional Sensing Model:

The 3D directional model is based on the FOV in WCSNs. As shown in Fig. 2, FOV for directional sensing model is defined as a cone with 4 tuples $\left(L_k, R_{k,s}, \overrightarrow{V_k}, \theta_k\right)$, where L_k is the location of the camera sensor k; $R_{k,s}$ is the sensing radius; $\overrightarrow{V_k}$ is the sensing direction; $\{-\theta_k, \theta_k\}$ is the offset angle on both sides of $\overrightarrow{V_k}$. In addition, the radius of the blind area is denoted as $R_{k,f}$. A target is said to be covered if and only if the following conditions hold:

(a) $R_{k,f} \leq d_{k,t} \leq R_{k,s}$;

(b) The offset angle between $\overrightarrow{L_k L_t}$ and $\overrightarrow{V_k}$ is within $[0, \theta_k]$.

Then, the directional sensing volume, denoted by V_k^{d}, can be derived as follows:

$$V_k^{\mathrm{d}} = \frac{2\pi\left(R_{k,s}^3 - R_{k,f}^3\right)(1 - \cos(\theta_k))}{3}. \tag{4}$$

B. 3D Sensor Deployment Model

The sensors are distributed as a stationary Poisson process with intensity of λ. The location of each sensor is independent and identically distributed (i.i.d.). Let k be a positive integer and N denote the number of camera sensors deployed in the 3D sensing space $\mathbf{V}$. We can derive the probability that there are k sensors in $\mathbf{V}$ as follows:

$$\Pr\{N = k\} = \frac{(\lambda\|\mathbf{V}\|)^k}{k!} e^{-\lambda\|\boldsymbol{V}\|}, \tag{5}$$

where $\|\mathbf{V}\|$ is the total volume of the 3D sensing space $\mathbf{V}$.

C. The Bond-Percolation Theory Based Model for Exposure-Path Prevention

As defined in [1], a continuous curve from one side of the deployment space to the opposite side is said to be an exposure path if the continuous curve belongs to a 3D vacant space which is not covered by any sensing sphere. According to percolation theory [12], we denote the *critical density* [13] of camera sensors by λ_c. If $\lambda \leq \lambda_c$, there exist exposure paths in the sensor-deployed space. The exposure-path problem is modeled by a 3D lattice with the length $2a$ of each axis, as shown in Fig. 3. The lattice contains M^3 vertexes with M vertexes along each axis of the lattice, denoted by $V_e = \{v_1, v_2, \ldots, v_{M^3}\}$. Let $e_{i,j}$ denote the edge

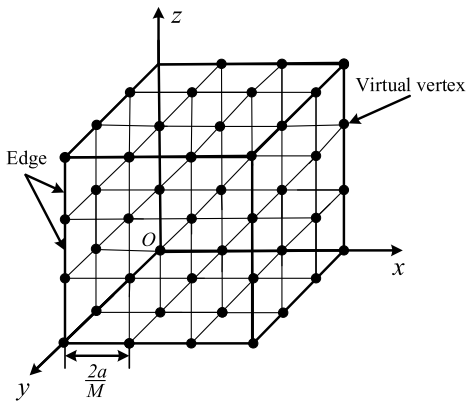

Fig. 3. 3D lattice for WCSNs.

between two vertexes v_i and v_j, where $i, j \in [1, 2, \ldots, M^3]$. Any two vertexes connected by a common edge are called the neighboring vertexes. The following two definitions is used to characterize whether edge $e_{i,j}$ is *open* or *closed*, which can yield the lower bound and upper bound of the critical density for 3D WCSNs:

Definition 1 (L-closed/L-open Edge): If at least one point on the edge $e_{i,j}$ is covered by a camera sensor network, then $e_{i,j}$ is said to be an *L-closed* edge. Otherwise, $e_{i,j}$ is called *L-open*.

Definition 2 (U-closed/U-open Edge): If all points on the edge $e_{i,j}$ are covered by a camera sensor network, then $e_{i,j}$ is called *U-closed*. Otherwise, $e_{i,j}$ is called *U-open*.

Define two functions to determine whether $e_{i,j}$ is closed or not. For *L-closed/L-open* edges, $L(e_{i,j}) = 1$, if at least one point on $e_{i,j}$ is covered; Otherwise, $L(e_{i,j}) = 0$. For *U-closed/U-open* edges, $U(e_{i,j}) = 1$, if all points on $e_{i,j}$ are covered; Otherwise, $U(e_{i,j}) = 0$. Then, we define the following two probabilities for *L-closed* edges and *U-closed* edges:

$$\begin{cases} p_l \triangleq \Pr\{L(e_{i,j}) = 1\}, \\ p_u \triangleq \Pr\{U(e_{i,j}) = 1\}. \end{cases} \tag{6}$$

Therefore, L-coverage lattice is applied to derive the *lower bound* of the critical density of the camera sensors, and U-coverage lattice is applied to derive the *upper bound* for the critical density of the camera sensors.

D. Nakagami-m Based Wireless Channel Model

We apply the Nakagami-*m* frequency-selective fading model [18], where m with $m \in [\frac{1}{2}, \infty)$ is the shape factor of the Nakagami-*m* model, in our proposed system. In the special case, $m = 1$ represents Rayleigh fading, and $m = \infty$ corresponds to the Gaussian channel. By applying our MIMO scheme, the frequency-selective channel can be converted into a parallel collection of frequency flat subchannels. The channel impulse response function, denoted by $h_{k,n}(t)$, between sensor node k and sensor node n can be expressed as follows:

$$h_{k,n}(t) = \sum_{q=0}^{Q-1} \alpha_{k,n}^{(q)} \delta\left(t - \tau_{k,n}^{(q)}\right) \exp\left(-\jmath \phi_{k,n}^{(q)}\right), \frac{1}{2} \le m < \infty \tag{7}$$

where $\jmath \triangleq \sqrt{-1}$; $\tau_{k,n}^{(q)}$ is the path delay, $\left\{\alpha_{k,n}^{(q)}\right\}$ is the path envelope, and $\left\{\phi_{k,n}^{(q)}\right\}$ is the phase-shift for the qth multi-path component of the channel, while Q is the total number of diverse channel paths. Assume that $\left\{\phi_{k,n}^{(q)}\right\}$ is i.i.d. random variables uniformly distributed between $[0, 2\pi)$, and $\left\{\alpha_{k,n}^{(q)}\right\}$ is i.i.d. random variables with Nakagami-*m* distribution. Nakagami's research shows that the signal amplitude fading in radio wave propagation can be well characterized by the following probability density function (PDF) [19],

$$f_\alpha(\alpha) = 2\left(\frac{m}{\Omega}\right)^m \frac{\alpha^{2m-1}}{\Gamma(m)} \exp\left(-m\frac{\alpha^2}{\Omega}\right), \tag{8}$$

where $\Omega = \mathbb{E}\{[\alpha]^2\}$ is the average path gain and $\Gamma(\cdot)$ denotes the Gamma function. Consequently, the received signal, denoted by $r_{k,n}(t)$, transmitted from camera sensor k to camera sensor n can be expressed as

$$r_{k,n}(t) = \sum_{q=0}^{Q-1} \sqrt{2\mathcal{P}_k}\alpha_{k,n}^{(q)} b\left(t - \tau_{k,n}^{(q)}\right) c\left(t - \tau_{k,n}^{(q)}\right) \times \exp\left[\jmath\left(2\pi f_c t + \varphi_{k,n}^{(q)}\right)\right] + n_{k,n}(t) \tag{9}$$

where $\varphi_{k,n}^{(q)} = -2\pi f_c \tau_{k,n}^{(q)} - \phi_{k,n}^{(q)}$; $\mathcal{P}_k$ is the transmit power at camera sensor k; f_c is the central frequency; $b(t - \tau_{k,n}^{(q)})$ denotes the transmitted symbol from camera sensor k to camera sensor n; $n_{k,n}(t)$ denotes the complex additive white Gaussian noise (AWGN) with zero mean and power spectral density of $N_0/2$; $c(t - \tau_{k,n}^{(q)})$ is the spread code which can be expressed as follows:

$$c(t) = \sum_{k=-\infty}^{+\infty} c[k] P_{T_c}(t - kT_c), \tag{10}$$

where $c[k]$ takes the values of $\{+1, -1\}$; $P_{T_c}(\cdot)$ stands for the unit rectangular-pulse function; T_c denotes the chip duration which follows $T_c = T_s/N_s$ with T_s being the symbol duration and N_s being the spreading gain.

III. The Critical Density of Camera Sensors

Assume that the probability whether all edges are closed or not is independent under bond-percolation theory. However, the $L\text{-}closed$ probability p_l and the $U\text{-}closed$ probability p_u of edge $e_{i,j}$ depend on the $L\text{-}closed$ probabilities and the $U\text{-}closed$ probabilities, respectively, of the neighboring edges in reality. The dependency issues will be analyzed in Section III-C. Define p_c to be the percolation threshold. For all $p > p_c$, there exists one closed path extending from one side to another, whereas for all $p < p_c$, there exists no exposure path. As proved in [20], percolation threshold p_c for 3D lattice is equal to 0.2488. Therefore, if $p_l < 0.2488$, there exist exposure paths; if $p_u > 0.2488$, there is no exposure path. The deployed camera sensor density, denoted by λ_l, for L-coverage lattice and λ_u for U-coverage lattice, respectively, are given as follows,

$$\begin{cases} \lambda_l \triangleq \sup\{\lambda \mid p_l \le 0.2488\}, \\ \lambda_u \triangleq \inf\{\lambda \mid p_u \ge 0.2488\}. \end{cases} \tag{11}$$

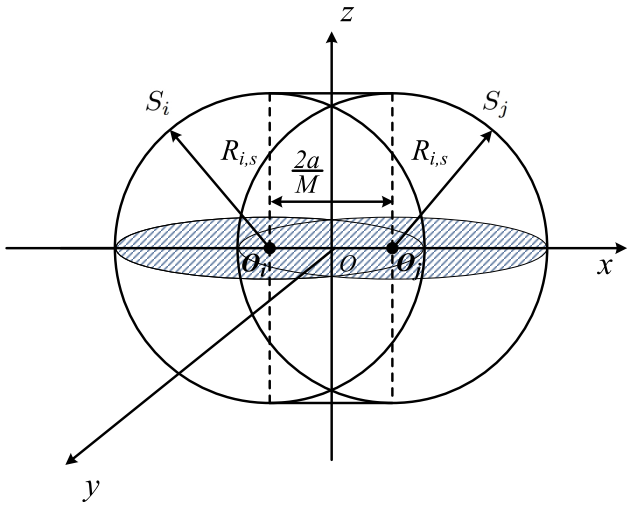

Fig. 4. The covered volume for edge $e_{i,j}$.

Then, define the critical density, denoted by λ_c, of camera sensors, satisfying the following inequations: $\lambda_l < \lambda_c < \lambda_u$.

A. The Critical Camera Sensor Density for Omnidirectional Model

Let t_n be any point on edge $e_{i,j}$. Define $S_i \bigsqcup S_j$ as follows:

$$S_i \bigsqcup S_j \triangleq \bigcup_{\forall t_n \in e_{i,j}} S_n, \tag{12}$$

where S_n is the sphere centered around t_n with radius $R_{k,s}$, as shown in Fig. 4; S_i is the sphere centered at O_i and S_j is the sphere centered at O_j. Assuming that all points on edge $e_{i,j}$ are not covered if and only if there is no sensor node within the space $S_i \bigsqcup S_j$, the deployed camera sensor density can be derived as in following equations [1]:

$$\begin{cases} \lambda_l = -\dfrac{\log(1-p_l)}{O^{\bigsqcup}}; \\ \lambda_u < -\dfrac{\log(1-p_u)}{O^{\bigcap}}, \end{cases} \tag{13}$$

where

$$\begin{cases} O^{\bigsqcup} = \dfrac{4}{3}\pi R_{k,s}^3 + 2\pi \dfrac{aR_{k,s}^2}{M}; \\ O^{\bigcap} = 8\displaystyle\int_{S_i \bigcap S_j} dv, \end{cases} \tag{14}$$

where we define $dv \triangleq dxdydz$; $O^{\bigsqcup}$ represents the volume of $S_i \bigsqcup S_j$ and $O^{\bigcap}$ denotes the volume of $S_i \bigcap S_j$. Consequently, using Eqs. (13) and (14), the lower bound and upper bound for critical density, denoted by λ_c^{o} of omnidirectional 3D sensing model are derived as follows:

$$\frac{-\log(1-p_l)}{\frac{4}{3}\pi R_{k,s}^2 + \frac{4aR_{k,s}}{M}} < \lambda_c^{\mathrm{o}} < \frac{-\log(1-p_u)}{O^{\bigsqcup}}. \tag{15}$$

B. The Critical Camera Sensor Density for Directional Model

Suppose there is a directional camera sensor at point L_k in $S_i \bigsqcup S_j$. A sphere centered at L_k with radius $R_{k,s}$ intersects x-axis at point $D_a \triangleq (x_k - \sqrt{R_{k,s}^2 - y_k^2 - z_k^2}, 0, 0)$ and $D_b \triangleq (x_k + \sqrt{R_{k,s}^2 - y_k^2 - z_k^2}, 0, 0)$. Let the Euclidean distance $d_{i,a} = \left| x_k - \sqrt{R_{k,s}^2 - y_k^2 - z_k^2} \right|$ and $d_{i,b} = x_k + \sqrt{R_{k,s}^2 - y_k^2 - z_k^2}$. Then, if $e_{i,j}$ is *L-closed*, the deployed camera sensor density for L-coverage lattice can be derived as follows [1]:

$$\lambda_l = \frac{-\log(1-p_l)}{\int_{S_i \bigsqcup S_j} \left(1 - p_n^{\bigsqcup}\right) dv}, \tag{16}$$

where $p_n^{\bigsqcup}$ denotes the probability that a directional camera sensor in $S_i \bigsqcup S_j$ cannot cover any point on $e_{i,j}$, which is given by the following equations:

$$p_n^{\bigsqcup} = \begin{cases} \dfrac{2\pi - 2\theta_k - \langle \overrightarrow{L_k v_i}, \overrightarrow{L_k D_b} \rangle}{2\pi}, & \text{if } d_{i,a} < -\dfrac{a}{M} \text{ and } |d_{i,b}| < \dfrac{a}{M}; \\ \dfrac{2\pi - 2\theta_k - \langle \overrightarrow{L_k D_a}, \overrightarrow{L_k D_b} \rangle}{2\pi}, & \text{if } -\dfrac{a}{M} < d_{i,a} < d_{i,b} < \dfrac{a}{M}; \\ \dfrac{2\pi - 2\theta_k - \langle \overrightarrow{L_k v_i}, \overrightarrow{L_k v_j} \rangle}{2\pi}, & \text{if } d_{i,a} < -\dfrac{a}{M} \text{ and } d_{i,b} > \dfrac{a}{M}; \\ \dfrac{2\pi - 2\theta_k - \langle \overrightarrow{L_k D_a}, \overrightarrow{L_k v_j} \rangle}{2\pi}, & \text{if } |d_{i,a}| < \dfrac{a}{M} \text{ and } d_{i,b} > \dfrac{a}{M}, \end{cases} \tag{17}$$

where $\langle \vec{x}, \vec{y} \rangle$ is defined as the angle between $\vec{x}$ and $\vec{y}$. Then, if $e_{i,j}$ is an arbitrary edge in U-coverage lattice in directional WCSNs, the probability for *U-closed* edges can be determined as follows [1],

$$p_u > 1 - \exp\left(-\lambda_u \int_{S_i \bigcap S_j} \left(1 - p_n^{\bigcap}\right) dv \right), \tag{18}$$

where the probability $p_n^{\bigcap}$ represents that the directional sensor in $S_i \bigcap S_j$ cannot cover any point on $e_{i,j}$, which can be expressed as follows:

$$p_n^{\bigcap} = \begin{cases} 1, & \text{if } \langle \overrightarrow{L_k v_i}, \overrightarrow{L_k v_j} \rangle > 2\theta_k; \\ \dfrac{2\pi - 2\theta_k - \langle \overrightarrow{L_k v_i}, \overrightarrow{L_k v_j} \rangle}{2\pi}, & \text{otherwise.} \end{cases} \tag{19}$$

Consequently, using Eq. (16), the lower and upper bounds for critical density, denoted by λ_c^{d}, of camera sensors can be derived as follows:

$$\frac{-\log(1-p_l)}{\int_{S_i \bigsqcup S_j} \left(1 - p_n^{\bigsqcup}\right) dv} < \lambda_c^{\mathrm{d}} < \frac{-\log(1-p_u)}{\int_{S_i \bigcap S_j} \left(1 - p_n^{\bigcap}\right) dv}. \tag{20}$$

C. Dependence Among Neighboring Edges

In reality, the $L\text{-}closed$ probability p_l and the $U\text{-}closed$ probability p_u of edge $e_{i,j}$ depend on the $L\text{-}closed$ probabilities and the $U\text{-}closed$ probabilities, respectively, of its neighboring edges. However, in bond-percolation theory, whether all edges are closed or not is independent. Accordingly, the dependency among neighboring edges need to be modeled

and analyzed. In our 3D sensing model, without loss of generality, consider edge $e_{1,2}$'s dependency on its neighboring edges. In particular, edge $e_{1,2}$ has 5 neighboring edges $e_{1,3}$, $e_{1,4}$, $e_{1,5}$, $e_{1,6}$ and $e_{1,7}$. According to [21] and [22], define n-variable *mutual entropy* which quantifies the amount of mutual information that is shared among n random variables. The n-variable mutual entropy is defined as follows:

$$I(X_1, X_2, \ldots, X_n) = \sum_{x_1 \in \varphi, x_2 \in \varphi, \ldots, x_n \in \varphi} P_{\mathbf{X}}(x_1, x_2, \ldots, x_n) \times \log \frac{P_{\mathbf{X}}(x_1, x_2, \ldots, x_n)}{\prod_{i=1}^{n} P_{X_i}(x_i)}, \quad (21)$$

where n-variable random vector $\mathbf{X} = (X_1, X_2, \ldots, X_n)$; $\varphi \in \{0, 1\}$; $P_{\mathbf{X}}(x_1, x_2, \ldots, x_n)$ is the joint probability mass function (PMF) of $X_1, X_1, \ldots, X_n$ and $P_{X_i}(x_i)$ is the marginal PMF of x_i, for $i = 1, 2, \ldots, n$. For L-coverage lattice with $n = 6$, see Fig. 3, we define

$$\begin{cases} P_{\mathbf{X}}(x_1, \ldots, x_6) = \Pr\{L(e_{1,2}) = x_1, \ldots, L(e_{1,7}) = x_6\}, \\ P_{X_1}(x_1) = \Pr\{L(e_{1,2}) = x_1\}, \\ \ldots \\ P_{X_6}(x_6) = \Pr\{L(e_{1,7}) = x_6\}, \end{cases} \quad (22)$$

where $x_1, \ldots, x_6 \in \varphi$.

As for n-variable mutual entropy $I(U(e_{1,2}), \ldots, U(e_{1,7}))$ for U-coverage lattice, the definitions are similar, but we use $P_{\mathbf{Y}}(y_1, \ldots, y_6)$ and $P_{Y_i}(y_i)$ instead, where $\mathbf{Y} = (Y_1, Y_2, Y_3, Y_4, Y_5, Y_6)$ and $y_1, \ldots, y_6 \in \varphi$. Then, $I(X_1, X_2, \ldots, X_6)$ for our omnidirectional model is calculated. From Eq. (14), for $i = 1, \ldots, 6$, we have

$$\begin{cases} P_{X_i}(0) = e^{-\lambda O^{\sqcup\!\sqcup}}, \\ P_{X_i}(1) = 1 - e^{-\lambda O^{\sqcup\!\sqcup}}. \end{cases} \quad (23)$$

Furthermore,

$$P_{\mathbf{X}}(0, 0, 0, 0, 0, 0) = \Pr\left\{ N\left(\bigsqcup_{i=1,\ldots,6} S_i = 0 \right) \right\}. \quad (24)$$

According to the identity for converting the joint distribution to the product of conditional distribution and marginal distribution, i.e., $P(AB) = P(A|B)P(B)$, the joint PMF of X_i, where $i = 1, 2, \ldots, 6$, can be determined. When $R_{k,s} = 10$, $a = 50$, and $n = 100$, we can observe from Fig. 5 that the maximum value for $I(L(e_{1,2}), L(e_{2,3}))$ is about 0.22 and the maximum value for $I(U(e_{1,2}), U(e_{2,3}))$ is about 0.26. Similarly, $I(X_1, X_2, \ldots, X_6)$ for directional model can be derived. Because of the large-scale feature for 3D WCSNs, there are a large number of camera sensors deployed in the entire sensing space. The mutual dependency among neighboring edges is relatively weak. Therefore, we can approximately apply the bond-percolation theory in our 3D sensing models.

IV. Energy Efficient DS-CDMA Based AQ-DBPSK Scheme

In large-scale WCSNs, because of the extremely large amount of sensor nodes, the interference among sensor nodes becomes significant, making the signal-to-interference-plus-noise ratio (SINR) [23] a key factor affecting the energy efficiency of the system. In clustered WCSNs, the communication is controlled by Media Access Control (MAC) protocol in order to minimize the interference during simultaneous communications among multiple sensor nodes, (cluster heads/cluster members). Among all the MAC protocols, DS-CDMA technique has been proved to be an effective way in significantly mitigating the interference and thus improving energy efficiency over WCSNs.

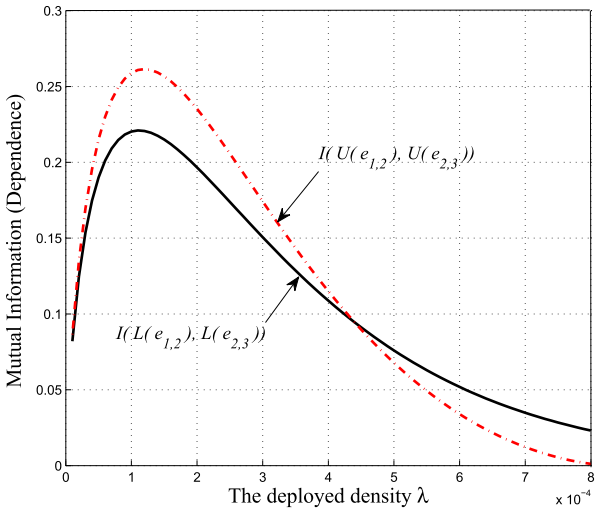

Fig. 5. Analysis and comparison between $I(L(e_{1,2}), \ldots, L(e_{1,7}))$ and $I(U(e_{1,2}), \ldots, U(e_{1,7}))$ for omnidirectional WCSNs.

In DS-CDMA scheme, we apply the correlator-based RAKE receiver in this paper. The RAKE receiver collects the signals from each multi-path, separates them, combines them, and then makes its own decision based on the combined strength of all signals present. In the RAKE receiver, we assume that the receiver has the perfect knowledge of the channel state information. Accordingly, the received signal, denoted by $Y_{k,n}$, at the receiver of the wireless channel between sensor node k and sensor node n can be derived as follows [11]:

$$Y_{k,n} = \int_0^{T_s} r_{k,n}(t) \alpha_{k,n}^{(\ell)} c\left(t - \tau_{k,n}^{(\ell)}\right) \exp\left[\jmath\left(2\pi f_c t + \varphi_{k,n}^{(\ell)}\right)\right] dt. \quad (25)$$

By substituting Eq. (9) into Eq. (25), we get

$$Y_{k,n} = T_s \sqrt{\frac{\mathcal{P}_k}{2}} \sum_{q=0}^{Q-1} \sum_{\ell=0}^{Q-1} \alpha_{k,n}^{(q)} \alpha_{k,n}^{(\ell)} R_{cc}\left(\tau_{k,n}^{(\ell)}\right) + N_{k,n}, \quad (26)$$

where

$$N_{k,n} = \sum_{\ell=0}^{Q-1} \int_0^{T_s} n_{k,n}(t) \alpha_{k,n}^{(\ell)} c\left(t - \tau_{k,n}^{(\ell)}\right) \times \exp\left[\jmath\left(2\pi f_c t + \varphi_{k,n}^{(\ell)}\right)\right] dt, \quad (27)$$

which is a Gaussian random variable with zero mean and variance of $T_s \sum_{\ell=0}^{Q-1} |\alpha_{k,n}^{(\ell)}|^2 N_0/2$, and $R_{cc}\left(\tau_{k,n}^{(\ell)}\right)$ is the auto-

correlation function defined as follows [24]:

$$R_{cc}\left(\tau_{k,n}^{(\ell)}\right) = \frac{1}{T_s}\int_0^{T_s} c(t)c\left(t-\tau_{k,n}^{(\ell)}\right)dt. \tag{28}$$

Correspondingly, we have

$$Y_{k,n} = T_s\sqrt{\frac{\mathcal{P}_k}{2}}\left(D_{k,n}+N_{k,n}+I_{k,n}\right), \tag{29}$$

where $D_{k,n}$ represents the desired output derived by substituting Eq. (9) into Eq. (25) and setting $q=\ell$ and $I_{k,n}$ is the multi-path interference given as follows:

$$I_{k,n} = \frac{\alpha_{k,n}^{(q)}\alpha_{k,n}^{(\ell)}\cos\left(\widetilde{\varphi}_{k,n}\right)R_{cc}\left(\tau_{k,n}^{(\ell)}\right)}{T_s}, \tag{30}$$

where $\widetilde{\varphi}_{k,n} = \varphi_{k,n}^{(q)} - \varphi_{k,n}^{(\ell)}$, which is a random variable uniformly in $[0, 2\pi)$. Then, since the multi-path interference $I_{k,n}$ can be approximated as a Gaussian random variable with zero mean, we can derive the variance of $I_{k,n}$ as follows:

$$\mathrm{Var}[I_{k,n}] = \frac{\Omega_{k,n}^{(\ell)}\alpha_{k,n}^{(\ell)}}{3N_s}, \tag{31}$$

where $\Omega_{k,n}^{(\ell)}$ denotes the second moment of $\alpha_{k,n}^{(\ell)}$, i.e., $\Omega_{k,n}^{(\ell)} = \mathbb{E}\left[\left(\alpha_{k,n}^{(\ell)}\right)^2\right]$. Consequently, the correlator output $Y_{k,n}$ in Eq. (29) can be approximated as a Gaussian random variable with normalized mean $D_{k,n}$ and normalized variance given as in the following equation:

$$\mathrm{Var}[Y_{k,n}] = \frac{\Omega_{k,n}^{(q)}\alpha_{k,n}^{(q)}}{3N_s} + \sum_{\ell=0,\ell\neq q}^{Q-1}\frac{\Omega_{k,n}^{(\ell)}\alpha_{k,n}^{(\ell)}}{3N_s}. \tag{32}$$

Furthermore, in order to further increase the energy efficiency, the simple but robust modulation technique called Alternating Quadratures Differential Binary Phase Shift Keying (AQ-DBPSK) [10] over Nakagami-*m* fading channel can be applied in our proposed 3D clustered WCSNs. AQ-DBPSK has been developed with the applications of the basic concepts for differential binary phase-shift keying (DBPSK) while maintaining all the advantages of DBPSK and eliminating its drawbacks. This is achieved by sending all the odd symbols in quadrature with the even symbols while the data is transmitted by the phase differences which are equal to 0° and 180° between same parity symbols. This operation achieves ±90° phase transition between all adjacent symbols. Consequently, it provides a low peak power, reducing the dynamic range of signal, and achieving a lower peak-to-average power ratio. Therefore, the more efficient power utilization is achieved in AQ-DBPSK than in DBPSK.

To model the performance of the AQ-DBPSK/DS-CDMA technique over 3D clustered WCSNs, first we need to derive the PDF of the signal-to-noise ratio (SNR) [9] as follows:

$$f_\gamma(\gamma) = \frac{\gamma^{m-1}}{\Gamma(m)}\left(\frac{m}{\overline{\gamma}}\right)^m\exp\left(-\frac{m\gamma}{\overline{\gamma}}\right), \tag{33}$$

where $\overline{\gamma}$ denotes the average SNR for qth path, $q = 0, 1, \ldots, (Q-1)$, which is given by the following equation [17]:

$$\overline{\gamma} = \frac{\Omega\mathcal{P}_k T_s}{N_0}, \tag{34}$$

where Ω is the average path gain specified by Eq. (8). Then, the joint PDF of the instantaneous SNR sequence $\{\gamma_{k,n}^{(q)}\}_{q=0}^{Q-1}$, that is, $f_{\gamma^{(0)},\gamma^{(1)},\ldots,\gamma^{(Q-1)}}\left(\gamma_{k,n}^{(0)},\gamma_{k,n}^{(1)},\ldots,\gamma_{k,n}^{(Q-1)}\right)$ can be derived. Assume that $\{\gamma_{k,n}^{(q)}\}_{q=0}^{Q-1}$ are independent [6]. Consequently, we have

$$f_{\gamma^{(0)},\gamma^{(1)},\ldots,\gamma^{(Q-1)}}\left(\gamma_{k,n}^{(0)},\gamma_{k,n}^{(1)},\ldots,\gamma_{k,n}^{(Q-1)}\right) = \prod_{q=0}^{Q-1} f_{\gamma^{(q)}}\left(\gamma_{k,n}^{(q)}\right). \tag{35}$$

In the AWGN channel, we can derive the bit error rate (BER), denoted by $P_b\left(\gamma_{k,n}\right)$, of the non-coherently demodulated AQ-DBPSK signals as follows [24]:

$$P_b(\gamma_{k,n}) = Q\left(\sqrt{\frac{\mathbb{E}[Y_{k,n}]}{\mathrm{Var}[Y_{k,n}]}}\right) = Q\left(\sqrt{2\sum_{q=0}^{Q-1}\gamma_{k,n}^{(q)}}\right), \tag{36}$$

where $\gamma_{k,n}^{(q)}$ denotes the SNR at qth multi-path and $Q(\cdot)$ is the Q-function. Finally, the BER of the multi-path channel model for DS-CDMA systems, denoted by $P_b(\gamma_{k,n}^{(q)})$, over Nakagami-*m* fading channel is derived as follows:

$$\begin{aligned}
P_b(\gamma_{k,n}^{(q)}) &= \int_0^\infty\int_0^\infty\cdots\int_0^\infty P_b(\gamma_{k,n})\prod_{q=0}^{Q-1} f_{\gamma^{(q)}}\left(\gamma_{k,n}^{(q)}\right) \\
&\quad\times d\gamma_{k,n}^{(0)}d\gamma_{k,n}^{(1)}\cdots d\gamma_{k,n}^{(Q-1)} \\
&= \frac{1}{\pi}\int_0^\infty\int_0^\infty\cdots\int_0^\infty\int_0^{\frac{\pi}{2}}\exp\left(\frac{-\sum_{q=0}^{Q-1}\gamma_{k,n}^{(q)}}{(\sin\theta)^2}\right)d\theta \\
&\quad\times\prod_{q=0}^{Q-1} f_{\gamma^{(q)}}(\gamma_{k,n}^{(q)})d\gamma_{k,n}^{(0)}d\gamma_{k,n}^{(1)}\cdots d\gamma_{k,n}^{(Q-1)} \\
&= \frac{1}{\pi}\int_0^{\frac{\pi}{2}}\prod_{q=0}^{Q-1} I_q\left(\overline{\gamma}_{k,n}^{(q)},\theta\right)d\theta,
\end{aligned} \tag{37}$$

where

$$I_q\left(\overline{\gamma}_{k,n}^{(q)},\theta\right) = \int_0^\infty\exp\left(-\frac{\overline{\gamma}_{k,n}^{(q)}}{(\sin\theta)^2}\right)f_{\gamma^{(q)}}(\overline{\gamma}_{k,n}^{(q)})d\overline{\gamma}_{k,n}^{(q)}, \tag{38}$$

and $\overline{\gamma}_{k,n}^{(q)}$ represents the average SNR over qth multi-path. Using the PDF of the SNR over Nakagami-*m* distribution in Eq. (33), we can show that

$$I_q\left(\overline{\gamma}_{k,n}^{(q)},\theta\right) = \left(\frac{m(\sin\theta)^2}{m(\sin\theta)^2+\overline{\gamma}_{k,n}^{(q)}}\right)^{mQ}, \tag{39}$$

where m is the parameter in the Nakagami-*m* distribution, specified by Eq. (8). Accordingly, by substituting Eq. (39) back into Eq. (37), we have

$$\begin{aligned}
P_b(\gamma_{k,n}^{(q)}) &= \frac{1}{\pi}\int_0^{\frac{\pi}{2}}\prod_{q=0}^{Q-1}\left(\frac{m(\sin\theta)^2}{m(\sin\theta)^2+\overline{\gamma}_{k,n}^{(q)}}\right)^{mQ}d\theta \\
&\le \frac{1}{\pi}\int_0^{\frac{\pi}{2}}\prod_{q=0}^{Q-1}\left(\frac{m}{m+\overline{\gamma}_{k,n}^{(q)}}\right)^{mQ}d\theta.
\end{aligned} \tag{40}$$

V. The Optimal Data Rate Control

For energy-efficient wireless communications over our proposed 3D clustered WCSNs, it is crucial to minimize the power consumption by controlling the available data transmission rate and applying the energy-efficiency optimization techniques. As shown in [25], we can derive the data transmission rate, denoted by $R_{k,n}$, for the reliable wireless data communications supported by the Nakagami-*m* fading channels over AQ-DBPSK/DS-CDMA based clustered WCSNs as follows:

$$R_{k,n} = W \log_2 (1+\gamma_{k,n}) = W \log_2 \left(1 + \frac{T_s \mathcal{P}_k \sum_{q=0}^{Q-1} |\alpha_{k,n}^{(q)}|^2}{N_0} \right), \tag{41}$$

where W is the bandwidth of each channel. Let the threshold of the data transmission rate to be R_{th} bits/sec. Then, the system is said to be in *outage* when

$$W \log_2 \left(1 + \frac{T_s \mathcal{P}_k \sum_{q=0}^{Q-1} \left| \alpha_{k,n}^{(q)} \right|^2}{N_0} \right) < R_{\text{th}}. \tag{42}$$

Assume that the power consumption of a camera node in transmission sensor mode consists of two parts. The first part is circuit power, denoted by $\mathcal{P}_{k,c}$, which is independent of data rate and present or exists whenever the user is in transmission mode. The second part is the transmit power which depends on the data rate. Authors of [26] show that the energy efficiency, denoted by $\eta_{k,n}$, for the communications between sensor nodes k and n can be defined as follows:

$$\eta_{k,n} = \frac{R_{k,n}}{\rho_k \mathcal{P}_k + \mathcal{P}_{k,c}}, \tag{43}$$

where ρ_k denotes the transmit power efficiency that scales up with the average transmit power due to amplifier loss. Accordingly, the operation of 3D WCSNs is optimized when the largest energy efficiency is achieved. Consequently, the optimal data rate can be determined as follows:

$$R_{k,n}^{\text{opt}} = \arg\max_{R_{k,n}} \{\eta_{k,n}\} = \arg\max_{R_{k,n}} \left\{ \frac{R_{k,n}}{\rho_k \mathcal{P}_k + \mathcal{P}_{k,c}} \right\}. \tag{44}$$

Using Eq. (41) and the relationship of $R_{k,n} = 1/T_s$, $\mathcal{P}_k$ can be derived as follows:

$$\mathcal{P}_k = \frac{\left(2^{\frac{R_{k,n}}{W}} - 1\right) N_0}{T_s \sum_{q=0}^{Q-1} \left| \alpha_{k,n}^{(q)} \right|^2} = \frac{\left(2^{\frac{R_{k,n}}{W}} - 1\right) N_0 R_{k,n}}{\sum_{q=0}^{Q-1} \left| \alpha_{k,n}^{(q)} \right|^2}, \tag{45}$$

which is a *monotonically increasing function* and *strictly convex* in $R_{k,n}$. Suppose $\mathcal{P}_k(0) = 0$. As proved in [27], if $\mathcal{P}_k$ is a monotonically increasing function and strictly convex in $R_{k,n}$, then there exists the unique globally optimal transmission data rate, denoted by $R_{k,n}^{\text{opt}}$. By taking the first-order derivative over Eq. (43), we have

$$\frac{\partial \eta_{k,n}}{\partial R_{k,n}} = \frac{\rho_k \mathcal{P}_k + \mathcal{P}_{k,c} - \frac{\partial \mathcal{P}_k}{\partial R_{k,n}} R_{k,n}}{\left(\rho_k \mathcal{P}_k + \mathcal{P}_{k,c}\right)^2} = 0, \tag{46}$$

which yields the following optimal solution for $R_{k,n}^{\text{opt}}$ satisfying the following equation:

$$R_{k,n}^{\text{opt}} = \frac{\rho_k \mathcal{P}_k + \mathcal{P}_{k,c}}{\frac{\partial \mathcal{P}_k}{\partial R_{k,n}^{\text{opt}}}}, \tag{47}$$

which maximizes the energy efficiency $\eta_{k,n}$ specified by Eq. (43). The optimal solution $R_{k,n}^{\text{opt}}$ will be used to determine the optimal data rate for each camera sensor to transmit the observed data, and also to derive the optimal symbol duration by using the following relationship:

$$T_s^{\text{opt}} = \frac{1}{R_{k,n}^{\text{opt}}}, \tag{48}$$

which will be applied back in Eqs. (10) and (34).

VI. The Cooperative MIMO Scheme for 3D Clustered WCSNs

In conventional WCSNs, because of the constraints of size and energy for each wireless camera sensor, there is usually one transmitter and one receiver applied at the wireless camera sensor. However, researchers have shown that it is possible to apply MIMO in WCSNs by using the cooperative techniques. In this section, the cooperative MIMO-LEACH technology [8] is applied to achieve the energy efficiency as well as the interference mitigation in long-haul data transmissions. In such cooperative MIMO wireless data transmissions, we apply the space-time block code (STBC) technology [28], [29] in order to achieve the spatial diversity.

A. The NEW LEACH Algorithm

Over the last decades, researchers have designed the low energy adaptive clustering hierarchy (LEACH) [30] algorithm in order to achieve energy efficiency over wireless sensor networks. The NEW LEACH algorithm proposed in [31] achieves better performance in energy saving and reducing the interference among the camera sensors over WCSNs. Compared with the traditional LEACH algorithm, NEW LEACH algorithm considers the different weights among residual energy, energy consumption rate, and location information, respectively.

According to NEW LEACH algorithm, at first all nodes has the same probability to become a cluster head. Let $\xi(k)$ denote the *threshold* whether camera sensor k can be selected as the cluster head. The decision is made at the beginning of each round by each node $k \in G$ independently choosing a random number in $[0, 1]$. If the random number is less than the threshold $\xi(k)$, then camera sensor k becomes a cluster head in the current round. The threshold $\xi(k)$ is derived as follows [16]:

$$\xi(k) = \begin{cases} \dfrac{p_\omega W_1 \frac{E_{k,c}}{E_{k,0}}}{1 - p_\omega \left(r \bmod \left(\frac{1}{p_\omega} \right) \right)} + \dfrac{p_\omega W_2 e^{-\frac{E_{k,b} - E_{k,c}}{E_{k,0}}}}{1 - p_\omega \left(r \bmod \left(\frac{1}{p_\omega} \right) \right)} \\ \quad + \dfrac{p_\omega W_3 \left(\frac{d_{avg}^2}{d_{\max}^2 + d_k^2} \right)}{1 - p_\omega \left(r \bmod \left(\frac{1}{p_\omega} \right) \right)}, & \text{if } \forall k \in G; \\ 0, & \text{otherwise,} \end{cases} \tag{49}$$

where G is the set of non-selected nodes in the previous rounds; r is the current round number per epoch; p_ω is the probability for a camera sensor to become a cluster head; $E_{k,0}$, $E_{k,c}$, and $E_{k,b}$ are the initial energy, current energy, and the energy in the former round comparing to the current round of the sensor node k, respectively; d_{avg} and $d_{\max}$ are the average distance and the maximum distance from the sensor nodes to the processing center, respectively; d_k is the distance from the current selected node to the processing center; $(W_1,\ W_2, W_3)$ are the weight values for the residual energy, energy consumption rate, and the location information. As shown in [6], the optimal combination of weights (W_1, W_2, W_3) is (0.111111, 0.000528, 0.88836), where $W_l > 0, \forall l \in \{1, 2, 3\}$ and $\sum_{l=1}^{3} W_l = 1$.

Then, we analyze the probability p_ω for a camera sensor to become a cluster head, specified in Eq. (49). The entire supervisory space is characterized as a cube with the side length of $2a$. According to [6], the optimal cluster head selection probability that minimizes the average total energy consumption over the entire 3D clustered WCSNs is derived as follows:

$$p_\omega^{\text{opt}} = \left\{ \frac{1}{11.532a\sqrt{\widetilde{\lambda}}} + \frac{0.109}{a\sqrt{\widetilde{\lambda}}\sqrt[3]{2+398.961a^2\widetilde{\lambda}+11.532\sqrt{3\widetilde{\lambda}(398.961a^2\widetilde{\lambda}+4)}}} + \frac{\sqrt[3]{2+398.961a^2\widetilde{\lambda}+11.532\sqrt{3\widetilde{\lambda}(398.961a^2\widetilde{\lambda}+4)}}}{11.532a\sqrt{\widetilde{\lambda}}\sqrt[3]{2}} \right\}^2 \tag{50}$$

where $\widetilde{\lambda} = \{\lambda_c^{\text{o}}, \lambda_c^{\text{d}}\}$ is the critical density for camera sensors deployed with $\widetilde{\lambda} = \{\lambda_c^{\text{o}}, \lambda_c^{\text{d}}\}$ given in Eqs. (15) and (20), respectively, and the optimal cluster head selection probability p_ω^{opt} can be used in Eq. (49) by setting $p_\omega = p_\omega^{\text{opt}}$.

B. Our Proposed Cooperative MIMO Schemes

Consider a multi-hop WCSNs with sensors grouped in cooperative clusters, as shown in Fig. 6. The ordinary nodes are the camera sensors that are not selected during the multihop data transmission. First, during the cluster formation phase, each camera sensor will elect itself to be a cluster head (CH) with the optimal cluster head selection probability p_ω^{opt} given in Eq. (50) based on our proposed NEW-LEACH algorithm. After the CHs are elected, each CH k will broadcast an advertisement message to the neighboring camera sensors with power $\mathcal{P}_k$. This message contains the CH's ID information. If another CH receives the advertisement message from CH_n and the received SNR exceeds certain threshold, the CH will be considered as a neighbor of CH_n. If a cluster member (CM_k) receives the advertisement message from CH_n and received SNR exceeds the threshold, CM_k will join the cluster

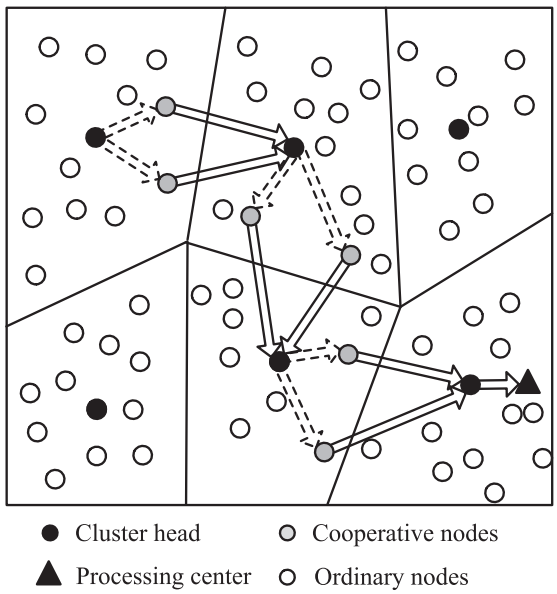

Fig. 6. Multi-hop MIMO-LEACH scheme.

by sending a join-request message back to CH_n. Once CH_n receives all the join-request messages, it will set up a time-division multiple access (TDMA) schedule and transmit it to all the CMs in the same cluster. In addition, if the processing center receives the advertisement message from the CHs, it will find the CH with maximum SNR, send its location message to the corresponding CH, and mark the CH as the target cluster head. Subsequently, we consider two kinds of clusters during each communication: transmitting cluster and receiving cluster [15]. The transmitting cluster is composed of a set of N_t cooperative sensor nodes, communicating with a receiving cluster composed of a set of N_r cooperative sensor nodes, where we assume that $\widetilde{M} = N_T = N_R$. During the transmission in each hop in a transmitting cluster, there are two main operations:

- *The Intracluster Communication Phase*: During the intracluster time slot 1 to τ, the cluster head (CH) k will broadcast the data bits to all cluster members (CMs) in the local cluster with power $\mathcal{P}_{k,1}$. The set of nodes falling into the broadcast capacity region will decode data and cooperate in the intercluster communication phase. The number of nodes belonging to the decoding set depends on the selection of $\mathcal{P}_{k,1}$. Among all the available nodes in the decoding set, $\widetilde{M}$ camera sensors with the best SNR will be selected to transmit in the next intercluster communications phase. The Nakagami-*m* flat fading channel is assumed for intracluster communications;
- *The Intercluster Communication Phase*: During the relay period $(\tau + 1)$ to 2τ, the subset of $\widetilde{M}$ CMs encode and jointly transmit the data bits to the CH in the next hop with power $\mathcal{P}_{k,2}$ according to the orthogonal linear STBC. We assume that the transmissions from each cooperative nodes experience Nakagami-*m* flat fading.

During the intercluster communication phase, the receiving cluster can receive data over virtual $N_t \times N_r$ MIMO channel, where N_t is the number of cooperative transmit antennas and

N_r represents the number of cooperative receive antennas. To improve the energy efficiency of the communications between CHs, appropriate strategies should be designed to choose the set of cooperative CMs in each hop. The selection diversity (SD) algorithm is applied as a reception protocol, that is, the receiver selects the nodes with the highest SNR to become the cooperative CMs, which can decode data and broadcast themselves during the intracluster communication in the next hop.

In any given cluster, the number cooperative CMs (i.e., the number of virtual transmit/receive antennas) is defined as $\widetilde{M} \triangleq N_t = N_r$. Assume that the channel state information is known at the receiver. There are $(L-1)$ hops connecting cluster 1 to cluster L through cluster $2, \ldots, (L-1)$. From the intracluster communication time slot 1 to τ, the selected cluster head k broadcasts signals to each cooperative CM. Then, from time slot $(\tau+1)$ to 2τ, the nth cooperative CM sends the information to the cluster head $\widetilde{k}$ in next hop. The received signal, denoted by $Z_{n,\widetilde{k}}^{(l+1)}$, at the CH $\widetilde{k}$ in the $(l+1)$th cluster corresponding to the cooperative multiple-input-single-output (MISO) channel, can be derived as follows:

$$Z_{n,\widetilde{k}}^{(l+1)} = h_{n,\widetilde{k}}^{(l)} Y_{n,\widetilde{k}}^{(l)} + W_{n,\widetilde{k}}^{(l)}, \tag{51}$$

where $h_{n,\widetilde{k}}^{(l)}$ is the Nakagami-m channel state information, as specified in Eq. (7); $Y_{n,\widetilde{k}}^{(l)}$ is the transmitted signal from the nth cooperative CM to CH $\widetilde{k}$; and $W_{n,\widetilde{k}}^{(l)}$ is the AWGN. Considering the STBC algorithm, we obtain:

$$\mathbf{Y}^{(\widetilde{k},l)} = \sqrt{\frac{\mathcal{P}_{k,2}}{\mathcal{P}_{k,1}+1}} \mathbf{B}^{(\widetilde{k},l)} \left[Y_{1,\widetilde{k}}^{(l)} Y_{2,\widetilde{k}}^{(l)} \cdots Y_{\widetilde{M},\widetilde{k}}^{(l)} \right]^T, \tag{52}$$

where $\mathbf{B}^{(\widetilde{k},l)}$ is a unitary matrix for the corresponding STBC block coding square matrix given as follows:

$$\mathbf{B}^{(\widetilde{k},l)} = \begin{bmatrix} b_{1,1}^{(\widetilde{k},l)} & \cdots & b_{1,\widetilde{M}}^{(\widetilde{k},l)} \\ \vdots & \ddots & \vdots \\ b_{\widetilde{M},1}^{(\widetilde{k},l)} & \cdots & b_{\widetilde{M},\widetilde{M}}^{(\widetilde{k},l)} \end{bmatrix}. \tag{53}$$

Combining Eqs. (51) and (52), we have

$$\mathbf{Z}^{(\widetilde{k},(l+1))} = \sqrt{\frac{\mathcal{P}_{k,1}\mathcal{P}_{k,2}\tau}{\mathcal{P}_{k,1}+1}} \mathbf{H}^{(\widetilde{k},l)} \mathbf{Y}^{(\widetilde{k},l)} + \mathbf{W}^{(\widetilde{k},l)}, \tag{54}$$

where

$$\begin{cases} \mathbf{H}^{(\widetilde{k},l)} = \begin{bmatrix} h_{1,\widetilde{k}}^{(l)} & & 0 \\ & \ddots & \\ 0 & & h_{\widetilde{M},\widetilde{k}}^{(l)} \end{bmatrix}; \\ \mathbf{W}^{(\widetilde{k},l)} = \left[W_{1,\widetilde{k}}^{(l)}, \ldots, W_{\widetilde{M},\widetilde{k}}^{(l)} \right]^T. \end{cases} \tag{55}$$

Therefore, the cooperative nodes generate the STBC $\mathbf{B}^{(\widetilde{k},l)}$ distributively and transmit the generated STBC $\mathbf{B}^{(\widetilde{k},l)}$ to the CH $\widetilde{k}$ in the lth cluster. Then, using Eq. (54), we can derive the SNR, denoted by $\gamma^{(\widetilde{k},l)}$, at the selection diversity receiver during lth hop as follows:

$$\gamma^{(\widetilde{k},l)} = \frac{2\mathcal{P}_{k,1}\mathcal{P}_{k,2}\tau}{(\mathcal{P}_{k,1}+1)N_0} \max\left\{ \left| h_{k,n}^{(l)} h_{n,\widetilde{k}}^{(l)} \right|^2 \right\}. \tag{56}$$

In the multi-hop wireless networks, the outage probability for multi-hop wireless communications, denoted by P_{out}, is evaluated in terms of the outage probability of every single hop, denoted by $P_{\text{out}}^{(l)}$, as follows:

$$P_{\text{out}} = 1 - \prod_{l=1}^{L-1} \left(1 - P_{\text{out}}^{(l)}\right). \tag{57}$$

In our proposed cooperative MIMO schemes, using the optimal CH selection probability p_ω^{opt} specified by Eq. (50), we can derive the outage probability of each single hop as follows:

$$P_{\text{out}}^{(l)} = \Pr\left\{ \sum_{\widetilde{k}=1}^{\widetilde{M}} p_\omega^{\text{opt}} \gamma^{(\widetilde{k},l)} \left| \mathbf{H}^{(\widetilde{k},l)} \right|^2 < 2^{\max\left\{R_{k,n}, R_{n,\widetilde{k}}\right\}} - 1 \right\} \tag{58}$$

where $R_{k,n}$ and $R_{n,\widetilde{k}}$ denote the data transmission rate for the intercluster communication phase and the intracluster communication phase, respectively; and $\gamma^{(\widetilde{k},l)}$ is specified in Eq. (56).

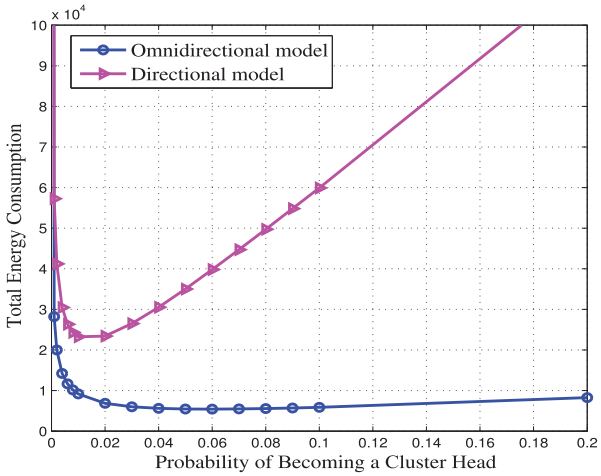

Fig. 7. Total energy consumption in 3D clustered WCSNs vs. probability of becoming a cluster head.

VII. Performance Evaluations

We use simulations to validate and evaluate our proposed schemes. We apply the non-cooperative clustering scheme and the Almouti scheme for performance comparison purpose. The parameters we use in our model are as follows: $R_{k,s} \in [5, 10]$ m, $R_{k,f} \in [0.05, 0.1]$ m, $\theta_k \in [\pi/6, \pi/4]$, $\mathbf{V} \in [50^3, 100^3]$ m^3, $E_0 = 0.5$ W, $\Gamma = 1$, and $Q = 100$.

Figure 7 depicts two curves of total energy consumption in the entire 3D clustered WCSNs for both omnidirectional and directional sensing models against the probability p_ω for a camera sensor to become a cluster head. From Fig. 7, we can observe that there exists an optimal probability p_ω^* that minimizes the total energy consumption in the 3D clustered WCSNs, which validates our schemes and also verifies the

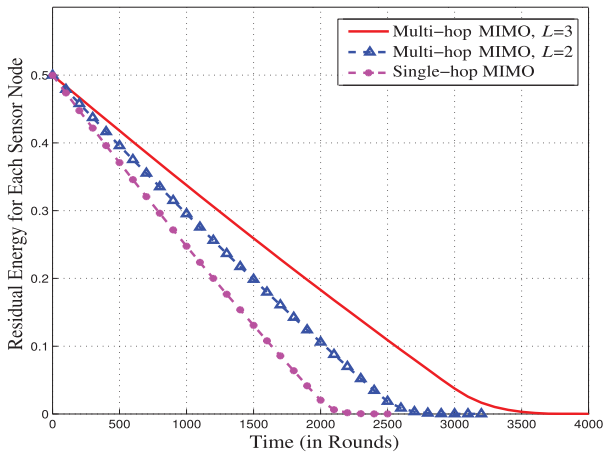

Fig. 8. Average residual energy for each camera sensor node with different number hops L.

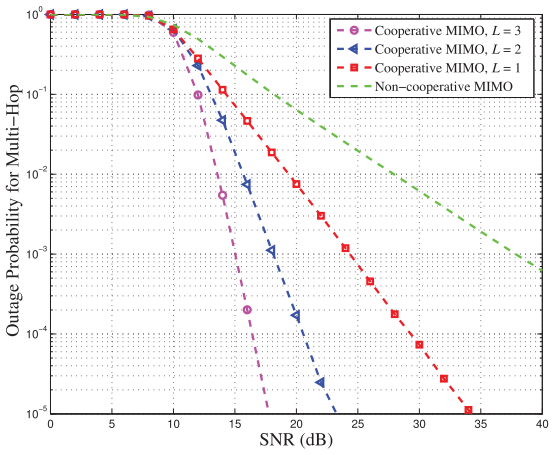

Fig. 10. Multi-hop outage probability vs. SNR (dB) over 3D clustered WCSNs with different number hops L.

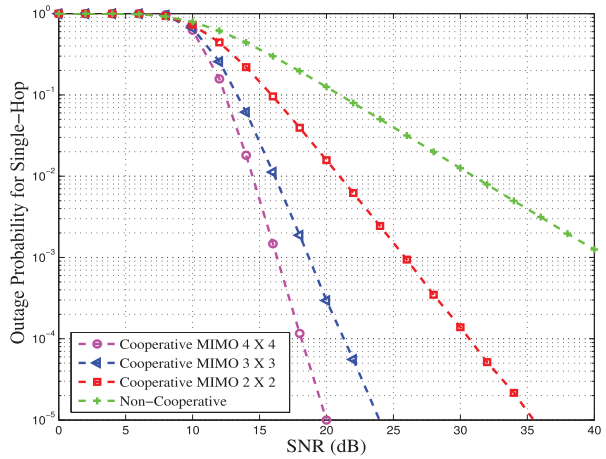

Fig. 9. Single hop outage probability vs. SNR (dB) over 3D clustered WCSNs.

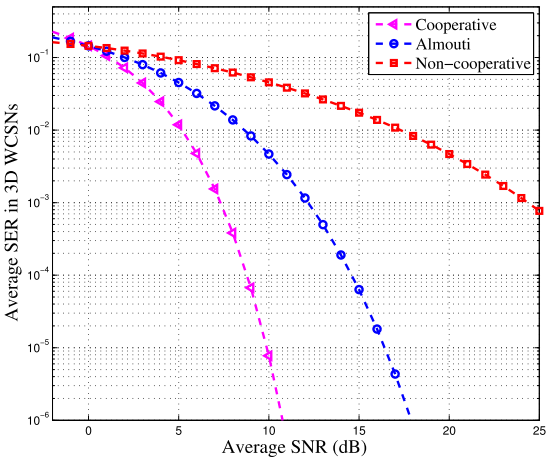

Fig. 11. Average symbol error rate (SER) in 3D WCSNs vs. average SNR (dB) over 3D clustered WCSNs.

correctness of derivations for Eq. (50) in our modeling and analyses.

Figure 8 plots the average residual energy for each camera sensor over time slots in 3D WCSNs. As illustrated in Fig. 8, we can observe that the proposed multi-hop scheme can significantly reduce the energy consumption for 3D WCSNs, which implies the importance of applying the multi-hop scheme in our proposed system. Fig. 8 also shows that the energy consumption can be reduced as the number of hops increases for our proposed 3D WCSNs.

Using Eq. (58), Fig. 9 compares four curves of the outage probability $P_{\text{out}}^{(l)}$ for single-hop transmission over the 3D clustered WCSNs against the SNR $\gamma^{(\widetilde{k},l)}$ with different number of cooperative CMs. Also, the outage probability of a non-cooperative MIMO system is shown in Fig. 9 for comparison. As illustrated in Fig. 9, we can observe that the outage probability of the cooperative MIMO gets better (decreases faster) when applying more cooperative nodes (more virtual antennas) in each hop, which achieves the same performance as in the real MIMO scheme.

Without loss of generality, we set $\widetilde{M} = N_t = N_r = 2$. Correspondingly, we can approximately achieve a 2×2 MIMO scheme, and the STBC block coding square matrix can be derived by setting the number of cooperative antennas $\widetilde{M} = 2$ for matrix $\mathbf{B}^{(\widetilde{k},l)}$ in Eq. (53). Then, using Eq. (57), Fig. 10 depicts the outage probability P_{out} of multi-hop communication against the SNR $\gamma^{(\widetilde{k},l)}$ for our proposed 2×2 scheme with various number of hops. The non-cooperate MIMO multi-hop case is plotted as a comparison reference. We can observe from Fig. 10 that as the value of SNR increases, the outage probability for our developed 3D scheme monotonically decreases, and when the parameter L for different number of hops increases, the outage probability gets better (decreases faster). When increasing the number of hops, the performance can be increased to very significant values. Moreover, in our proposed cooperative MIMO-LEACH scheme over 3D multi-hop clustered WCSNs, the value of SNR is increased because of the use of the cooperative MIMO technique and the clustering algorithm. As a result, with increased SNR, the outage probability can be significantly decreased for our developed scheme.

Compared with the existing 2×2 Almouti and non-cooperative schemes, Fig. 11 plots the average SER against the average SNR for our developed 2×2 cooperative MIMO-

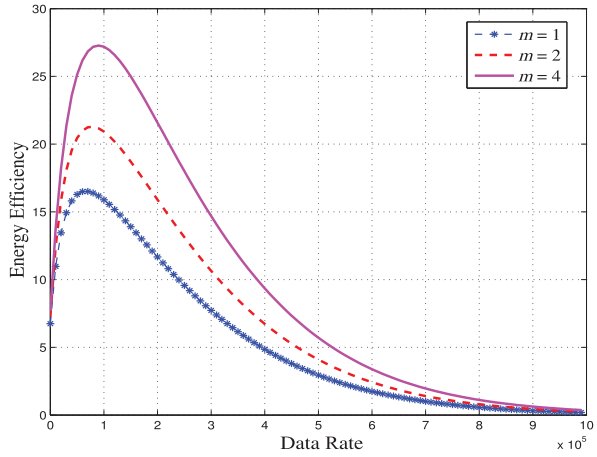

Fig. 12. Energy efficiency vs. data rate in 3D clustered WCSNs.

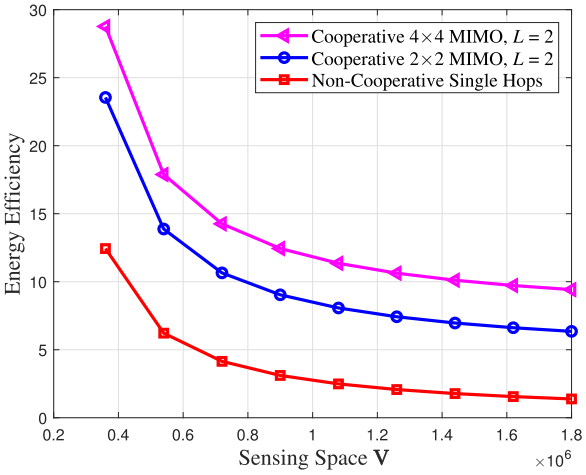

Fig. 14. Energy efficiency vs. sensing space $\mathbf{V}$ in 3D clustered WCSNs.

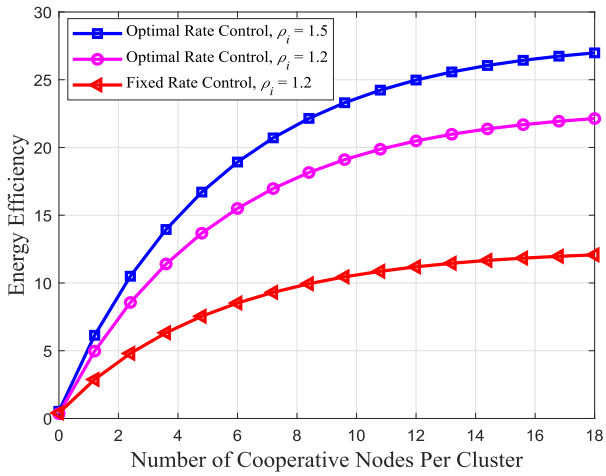

Fig. 13. Energy efficiency vs. number of cooperative nodes per cluster in 3D clustered WCSNs.

LEACH scheme over Nakagami-m wireless channel in 3D clustered WCSNs. Fig. 11 clearly shows that the SER curve for our proposed cooperative MIMO-LEACH scheme is much lower than those for Almouti and non-cooperative schemes, implying that our developed scheme significantly outperforms the Almouti and non-cooperative schemes in terms of average SER caused/affected by interferences and energy efficiency.

Using Eq. (43) and Eq. (45), Fig. 12 plots the energy efficiency against the transmission data rate with different Nakagami-m model parameter m. From Fig. 12, we can observe that the energy efficiency is not a monotonic function of transmission data rate and instead, there exists a maximum value for energy efficiency for any given m, which corresponds to the optimal data rate $R_{k,n}^{\text{opt}}$, verifying the correctness of derivation of Eq. (47). This implies that if the data rate is too small, then the energy efficiency decreases because we do not make the best use of the system resources; on the other hand, if the data rate is too large, then the energy efficiency also drops because of the impact of interference and increased BER. Then, by deriving and seeking the optimal data rate, we can achieve the optimal/maximum energy efficiency. From above observations, our proposed schemes outperform other existing schemes in terms of energy-efficiency and interference-mitigation subject to the minimum coverage rate constraint over 3D clustered WCSNs.

Compared with the fixed-rate control policy, Fig. 13 plots the energy efficiency against the number of cooperative nodes in each cluster. We can observe from Fig. 13 that our proposed optimal rate control policy suffers much less energy-efficiency loss as compared with the fixed rate control policy. Fig. 13 also shows that the optimal rate control can maximize the energy efficiency for our proposed 3D WCSNs. In addition, Fig. 14 plots the energy efficiency against the sensing space $\mathbf{V}$. We can observe from Fig. 14 that the energy efficiency decreases as the sensing space $\mathbf{V}$ increases. Also, Fig. 14 shows that our proposed cooperative MIMO schemes outperform the non-cooperative single-hop scheme in terms of energy efficiency over 3D WCSNs.

VIII. Conclusions

We proposed the AQ-DBPSK/DS-CDMA based cooperative MIMO scheme for energy-efficiency and interference mitigation subject to the minimum coverage rate constraint in our developed multi-hop 3D clustered WCSNs. First, we built the sensing models to characterize the minimum coverage rate constraint, formulated the exposure-path prevention problem under the percolation theory, and established the wireless channel model using Nakagami-m distribution. Then, we derived the critical density of camera sensors subject to the minimum exposure-path prevention probability constraint using bond-percolation theory. We developed the AQ-DBPSK/DS-CDMA scheme to implement the energy-efficient and interference-mitigation wireless communications over our proposed 3D clustered WCSNs. Furthermore, we derived the optimal data rate to optimize the transmit-power and data-rate trade-off for each camera sensor. For the required minimum coverage rate constraint of 3D clustered WCSNs, we applied the cooperative MIMO based NEW LEACH architecture to derive the optimal probability of selecting cluster heads for minimizing energy consumption and interference among multiple camera

sensors. Then, using the Nakagami-m model, we developed the multi-hop cooperative MIMO scheme to achieve the energy efficient and interference-mitigating wireless communications over our proposed 3D clustered WCSNs. Also conducted was a set of simulation evaluations which show that our proposed scheme can outperform the other existing schemes in terms of energy efficiency and interference-mitigation over 3D clustered WCSNs.

REFERENCES

[1] J. Wang and X. Zhang, "3D percolation theory-based exposure-path prevention for optimal power-coverage tradeoff in clustered wireless camera sensor networks," in *Proc. IEEE Global Commun. Conf. (GLOBECOM)*, Austin, TX, USA, Dec. 2014, pp. 305–310.

[2] L. Liu, X. Zhang, and H. Ma, "Optimal density estimation for exposure-path prevention in wireless sensor networks using percolation theory," in *Proc. IEEE INFOCOM*, Baltimore, MD, USA, Mar. 2012, pp. 2601–2605.

[3] L. Liu, X. Zhang, and H. Ma, "Percolation theory-based exposure-path prevention for wireless sensor networks coverage in Internet of Things," *IEEE Sensor J.*, vol. 13, no. 10, pp. 3625–3636, Oct. 2013.

[4] J. W. Essam, "Percolation theory," *Rep. Progr. Phys.*, vol. 43, no. 7, pp. 833–912, 1980.

[5] S. Bandyopadhyay and E. J. Coyle, "An energy efficient hierarchical clustering algorithm for wireless sensor networks," in *Proc. 22nd Annu. Joint Conf. IEEE Comput. Commun. (INFOCOM)*, Apr. 2003, pp. 1713–1723.

[6] L. Xie and X. Zhang, "3D clustering-based camera wireless sensor networks for maximizing lifespan with minimum coverage rate constraint," in *Proc. IEEE GLOBECOM*, Atlanta, GA, USA, Dec. 2013, pp. 298–303.

[7] Y. Jing and B. Hassibi, "Distributed space-time coding in wireless relay networks," *IEEE Trans. Wireless Commun.*, vol. 5, no. 12, pp. 3524–3536, Dec. 2006.

[8] Y. Yuan, Z. He, and M. Chen, "Virtual MIMO-based cross-layer design for wireless sensor networks," *IEEE Trans. Veh. Technol.*, vol. 55, no. 3, pp. 856–864, May 2006.

[9] L.-L. Yang and L. Hanzo, "Performance of generalized multicarrier DS-CDMA over Nakagami-m fading channels," *IEEE Trans. Commun.*, vol. 50, no. 6, pp. 956–966, Jun. 2002.

[10] Y. S. Poberezhskiy, "Novel modulation techniques and circuits for transceivers in body sensor networks," *IEEE J. Emerg. Sel. Topics Circuits Syst.*, vol. 2, no. 1, pp. 96–108, Mar. 2012.

[11] J. Wang and X. Zhang, "AQ-DBPSK/DS-CDMA based energy-efficient and interference-mitigation scheme for 3D clustered WCSNs with minimum coverage rate constraint," in *Proc. IEEE MILCOM*, Baltimore, MD, USA, Oct. 2014, pp. 305–310.

[12] L. Liu, X. Zhang, and H. Ma, "Bond-percolation based optimal density for exposure-path prevention in wireless sensor networks," in *Proc. IEEE GLOBECOM 2008*, Nov. 2008, pp. 1–5.

[13] H. M. Ammari and S. K. Das, "Critical density for coverage and connectivity in three-dimensional wireless sensor networks using continuum percolation," *IEEE Trans. Parallel Distrib. Syst.*, vol. 20, no. 6, pp. 872–885, Jun. 2009.

[14] L. Liu, X. Zhang, and H. Ma, "Optimal node selection for target localization in wireless camera sensor networks," *IEEE Trans. Veh. Technol.*, vol. 59, no. 7, pp. 3562–3576, Sep. 2013.

[15] A. Del Coso, U. Spagnolini, and C. Ibars, "Cooperative distributed MIMO channels in wireless sensor networks," *IEEE J. Sel. Areas Commun.*, vol. 25, no. 2, pp. 402–414, Feb. 2007.

[16] J. Wang and X. Zhang, "Cooperative MIMO-OFDM based multi-hop 3D clustered wireless camera sensor networks," in *Proc. IEEE Wireless Commun. Netw. Conf. (WCNC)*, New Orleans, LA, USA, Mar. 2015, pp. 1350–1355.

[17] J. Tang and X. Zhang, "Transmit selection diversity with maximal-ratio combining for multicarrier DS-CDMA wireless networks over Nakagami-m fading channels," *IEEE J. Sel. Areas Commun.*, vol. 24, no. 1, pp. 104–112, Jan. 2006.

[18] N. C. Beaulieu and C. Cheng, "Efficient Nakagami-m fading channel simulation," *IEEE Trans. Veh. Technol.*, vol. 54, no. 2, pp. 413–424, Mar. 2005.

[19] F. Lopez-Martinez, D. Morales-Jimenez, E. Martos-Naya, and J. F. Paris, "On the bivariate Nakagami-m cumulative distribution function: Closed-form expression and applications," *IEEE Trans. Commun.*, vol. 61, no. 4, pp. 1404–1414, Apr. 2012.

[20] J. Wang, Z. Zhou, W. Zhang, T. M. Garoni, and Y. Deng, "Bond and site percolation in three dimensions," *Phys. Rev. E, Stat. Phys. Plasmas Fluids Relat. Interdiscip. Top.*, vol. 87, no. 5, May 2013, Art. no. 052107.

[21] M. Studený and J. Vejnarová, "The multiinformation function as a tool for measuring stochastic dependence," in *Learning in Graphical Models*, MIT Press, Cambridge, vol. 89. 1998, pp. 261–297.

[22] T. V. de Cruys, "Two multivariate generalizations of pointwise mutual information," in *Proc. Workshop Distrib. Semantics Compositionality (DiSCo)*, Stroudsburg, PA, USA, 2011, pp. 16–20.

[23] O. Dousse, F. Baccelli, and P. Thiran, "Impact of interferences on connectivity in ad hoc networks," in *Proc. IEEE INFOCOM*, Mar./Apr. 2003, pp. 2791–2795.

[24] A. Goldsmith, *Wireless Communications*. Cambridge, U.K.: Cambridge Univ. Press, 2005.

[25] D. Tse and P. Viswanath, *Fundamentals of Wireless Communication*. Cambridge, U.K.: Cambridge Univ. Press, 2005.

[26] G. Miao, N. Himayat, G. Y. Li, A. T. Koc, and S. Talwar, "Interference-aware energy-efficient power optimization," in *Proc. IEEE ICC*, Dresden, Germany, Jun. 2009, pp. 1–5.

[27] G. Miao, N. Himayat, G. Y. Li, and D. Bormann, "Energy efficient design in wireless OFDMA," in *Proc. IEEE ICC*, Beijing, China, May 2008, pp. 3307–3312.

[28] D. A. Gore and A. J. Paulraj, "MIMO antenna subset selection with space-time coding," *IEEE Trans. Signal Process.*, vol. 50, no. 10, pp. 2580–2588, Oct. 2002.

[29] F. T. Alotaibi and J. A. Chambers, "Extended orthogonal space time block codes in wireless relay networks," in *Proc. IEEE/SP 15th Workshop Trans. Stat. Signal Process.*, Aug./Sep. 2009, pp. 745–748.

[30] W. B. Heinzelman, A. P. Chandrakasan, and H. Balakrishnan, "An application-specific protocol architecture for wireless microsensor networks," *IEEE Trans. Wireless Commun.*, vol. 1, no. 4, pp. 660–670, Oct. 2002.

[31] G. Smaragdakis, I. Matta, and A. Besravros, "SEP: A stable election protocol for clustered heterogeneous wireless sensor networks," Dept. Comput. Sci., Boston Univ., Boston, MA, USA, Tech. Rep. BUCS-TR-2004-022, 2004.

Jingqing Wang received the B.S. degree in electronics and information engineering from Northwestern Polytechnical University, Xi'an, China. She is currently pursuing the Ph.D. degree with the Networking and Information Systems Laboratory, Department of Electrical and Computer Engineering, Texas A&M University, College Station, TX, USA under the supervision of Professor Xi Zhang.

Her research interests focus on big data-based 5G wireless networks technologies, statistical QoS provisioning, and cognitive radio networks.

Ms. Wang has received the Best Paper Award from IEEE GLOBECOM 2014 and the Hagler Institute for Advanced Study HEEP Graduate Fellowship Award from Texas A&M University, College Station, TX, USA, in 2018.

Xi Zhang (S'89–SM'98–F'16) received the B.S. and M.S. degrees from Xidian University, Xi'an, China, the M.S. degree from Lehigh University, Bethlehem, PA, USA, all in electrical engineering and computer science, and the Ph.D. degree in electrical engineering and computer science (Electrical Engineering-Systems) from The University of Michigan, Ann Arbor, MI, USA.

He is currently a Full Professor and the Founding Director of the Networking and Information Systems Laboratory, Department of Electrical and Computer Engineering, Texas A&M University, College Station. He is a Fellow of the IEEE for contributions to quality of service (QoS) theory in mobile wireless networks. He was with the Networks and Distributed Systems Research Department, AT&T Bell Laboratories, Murray Hill, NJ, USA, and AT&T Laboratories Research, Florham Park, NJ, USA, in 1997. He was a Research Fellow with the School of Electrical Engineering, University of Technology Sydney, Australia, and the Department of Electrical and Computer Engineering, James Cook University, Australia. He has published more than 330 research papers on wireless networks and communications systems, network protocol design and modeling, statistical communications, random signal processing, information theory, and control theory and systems. He received the U.S. National Science Foundation CAREER Award in 2004 for his research in the areas of mobile wireless and multicast networking and systems. He received five Best Paper Awards at IEEE ICC 2018, IEEE GLOBECOM 2014, IEEE GLOBECOM 2009, IEEE GLOBECOM 2007, and IEEE WCNC 2010, respectively. One of his IEEE JOURNAL ON SELECTED AREAS IN COMMUNICATIONS papers has been listed as the IEEE Best Readings Paper (receiving the highest citation rate among all IEEE Transactions/Journal papers in the area) on Wireless Cognitive Radio Networks and Statistical QoS Provisioning over Mobile Wireless Networking. He is an IEEE Distinguished Lecturer of both IEEE Communications Society and IEEE Vehicular Technology Society. He also received the TEES Select Young Faculty Award for Excellence in Research Performance from the Dwight Look College of Engineering at Texas A&M University in 2006.

Professor Zhang is serving or has served as an Editor for IEEE TRANSACTIONS ON COMMUNICATIONS, IEEE TRANSACTIONS ON WIRELESS COMMUNICATIONS, IEEE TRANSACTIONS ON VEHICULAR TECHNOLOGY, IEEE TRANSACTIONS ON GREEN COMMUNICATIONS AND NETWORKING, and IEEE TRANSACTIONS ON NETWORK SCIENCE AND ENGINEERING, twice as a Guest Editor for IEEE JOURNAL ON SELECTED AREAS IN COMMUNICATIONS for two special issues on "Broadband Wireless Communications for High Speed Vehicles" and "Wireless Video Transmissions," an Associate Editor for IEEE COMMUNICATIONS LETTERS, twice as the Lead Guest Editor for *IEEE Communications Magazine* for two special issues on "Advances in Cooperative Wireless Networking" and "Underwater Wireless Communications and Networks: Theory and Applications," a Guest Editor for *IEEE Wireless Communications Magazine* for special issue on "Next Generation CDMA versus OFDMA for 4G Wireless Applications," an Editor for *Journal on Wireless Communications and Mobile Computing* (Wiley), the *Journal of Computer Systems, Networking, and Communications*, and *Journal on Security and Communications Networks* (Wiley), and an Area Editor for *Journal on Computer Communications* (Elsevier), among many others. He is serving or has served as the TPC Chair for IEEE GLOBECOM 2011, TPC Vice-Chair for IEEE INFOCOM 2010, TPC Area Chair for IEEE INFOCOM 2012, Panel/Demo/Poster Chair for ACM MobiCom 2011, General Chair for IEEE WCNC 2013, and TPC Chair for IEEE INFOCOM 2017–2019 Workshops on "Integrating Edge Computing, Caching, and Offloading in Next Generation Networks," etc.